Published in final edited form as:
J Thromb Haemost. 2011 July ; 9(7): 1292–1300. doi:10.1111/j.1538-7836.2011.04339.x.

Thrombin-inhibiting perfluorocarbon nanoparticles provide a novel strategy for treatment and magnetic resonance imaging of acute thrombosis

J. Myerson, **L. He**, **G. Lanza**, **D. Tollefsen**, and **S. Wickline**
Washington University in Saint Louis, Biomedical Engineering, Saint Louis, MO, USA

Abstract

Background—As a regulator of the penultimate step in the coagulation cascade, thrombin represents a principal target of direct and specific anticoagulants.

Objective—A potent thrombin inhibitor complexed with a colloidal nanoparticle was devised as a first-in-class anticoagulant with prolonged and highly localized therapeutic impact conferred by its multivalent thrombin-absorbing particle surface.

Methods—PPACK (Phe(D)-Pro-Arg-Chloromethylketone) was secured covalently to the surface of perfluorocarbon-core nanoparticle structures. PPACK and PPACK nanoparticle inhibition of thrombin were assessed in vitro via thrombin activity against a chromogenic substrate. In vivo antithrombotic activity of PPACK, heparin, non-functionalized nanoparticles, and PPACK nanoparticles was assessed through IV administration prior to acute photochemical injury of the common carotid artery. Perfluorocarbon particle retention in extracted carotid arteries from injured mice was assessed via 19F magnetic resonance spectroscopy (MRS) and imaging (MRI) at 11.7 T. APTT measurements determined the systemic effects of the PPACK nanoparticles at various times after injection.

Results—Optical assay verified that PPACK nanoparticles exceeded PPACK's intrinsic activity against thrombin. Application of the an *in vivo* acute arterial thrombosis model demonstrated that PPACK nanoparticles outperformed both heparin (p=.001) and uncomplexed PPACK (p=.0006) in inhibiting thrombosis. 19F MRS confirmed that PPACK nanoparticles specifically bound to sites of acute thrombotic injury. APTT normalized within twenty minutes of PPACK nanoparticles injection.

Conclusions—PPACK nanoparticles present thrombin-inhibiting surfaces at sites of acutely forming thrombi that continue to manifest local clot inhibition even as systemic effects rapidly diminish and thus represent a new platform for localized control of acute thrombosis.

Keywords

imaging; inhibitors; nanotechnology; pharmacology; thrombin; thrombosis

Introduction

The acute onset of localized thrombosis in the coronary and carotid arteries is the proximate cause of heart attack and stroke, which typically are treated with a cocktail of various

Correspondence: Jacob Myerson, Washington University in Saint Louis, Biomedical Engineering, 4320 Forest Park Avenue, Suite 101, Saint Louis, MO 63108, USA, Tel.: + 1 617 5962715; fax: + 1 314 4547490. cleghorn@alum.mit.edu.

Disclosures
Samuel A. Wickline and Gregory M. Lanza are equity holders and consultants with Kereos, Inc.

anticoagulants and antiplatelet agents administered orally and intravenously to prevent further clot progression[1–9]. Yet even with aggressive regimens, thrombus formation still proceeds unpredictably[2,3,4,7]. Conversely, severe bleeding problems can arise using the current array of systemically active anticoagulants[3,5,6,7,]. Furthermore, stuttering thrombosis and microembolization can affect the assessment of outcomes with current treatment strategies[4]. Thus the development of safer and more effective anticoagulants remains an active pharmaceutical pursuit pertinent to the control of thrombotic events in acute vascular syndromes[3,5–12].

We hypothesized that inherently anticoagulant nanoparticulate structures not only could offer a safer and more efficacious platform for localized antithrombotic action, but simultaneously could provide a means to detect an acute thrombotic event in a culprit artery or vein due to their ability to be imaged[13,14]. Although nanoparticles have been suggested as a means of conveying common anticoagulants to vascular segments[15], it has not been shown that they would function as effective antithrombotics in vivo. Here, a perfluorocarbon-core (PFC) nanoparticle[16,17] is demonstrated as an integrated antithrombotic where the nanoparticle itself plays a critical role in preventing coagulation by presenting thrombin-absorbing surfaces at the site of vascular injury.

The central role of thrombin as a rate-limiting factor in clotting and platelet activation[12,18–24] motivated the design of an anticoagulant nanoparticle that could achieve high affinity molecular targeting of thrombin at sites of acute thrombosis. The nanoparticle surface is activated against thrombin by permanent covalent attachment of D-phenylalanyl-L-prolyl-L-arginyl-chloromethyl ketone (PPACK), a highly effective irreversible thrombin inhibitor with sub-nanomolar affinity for thrombin and several orders of magnitude lower affinity for similar proteases[10,12,18,19,25]. PPACK in complex with thrombin has a well-characterized stable structure[12,18,19]. It has an excellent safety profile in vivo, with an LD_{50} greater than 50 mg/kg and no long-term toxicity in mice[10,26], but its pharmacokinetics are unfavorable for antithrombotic use in vivo due to rapid elimination (~3 minutes half-life).

Thus, the present antithrombotic nanoparticle was designed to manifest prolonged local bioactivity against clotting, in the face of very rapid attenuation of systemic anticoagulation to achieve an improved safety profile. Additionally, we show that the particle can be detected specifically and quantitatively as it accumulates at the site of activated thrombin with the use of magnetic resonance imaging and spectroscopy of its fluorine (^{19}F) core. In this manner, acute thrombosis can be identified by direct molecular targeting of thrombin, which concomitantly results in its inhibition.

Methods

Nanoparticle Synthesis

PFC nanoparticles were prepared as described in previous work[27]. The emulsions contained 20% (vol/vol) Perfluoro 15-Crown-5 Ether (Exfluor Research Corp.), 2% (wt/vol) of a surfactant mixture, 1.7% (wt/vol) glycerin, and water for the balance. The surfactant, including 98.5 mole% phosphatidylethanolamine (Avanti Polar Lipids) and 1.5 mole% 1,2-distearoyl-sn-glycero-3-phosphoethanolamine-N-[carboxy(polyethylene glycol)-2000] (Avanti Polar Lipids) or 98 mole% egg yolk phosphotidylcholine (Avanti Polar Lipids) and 2 mole% phosphatidylethanolamine (Avanti Polar Lipids) in chloroform:methanol (3:1), was dried under vacuum to form a lipid film. The surfactant components were combined with the crown ether and distilled de-ionized water, and emulsified (Microfluidics Inc) at 20000 psi for 4 minutes. Particle sizes were measured immediately after synthesis using a laser light scattering submicron particle analyzer (Brookhaven Instruments).

Amine-carboxyl coupling was employed to functionalize particles containing 1,2-distearoyl-sn-glycero-3-phosphoethanolamine-N-[carboxy(polyethylene glycol)-2000] with PPACK. After one hour mixing of 1 mL emulsion with 12.5 mg PPACK, EDCI 1-[3-(Dimethylamino)propyl]-3-ethylcarbodiimide methiodide (2 mg) was added for overnight coupling. Excess PPACK and EDCI was removed by dialysis (MWCO 3000–5000). Particle size was assessed before and after PPACK conjugation. Extent of PPACK coupling was determined by reverse-phase HPLC quantification of uncoupled PPACK after centrifugation of nanoparticles with Cleanascite lipid adsorption reagent (Agilent Technologies). Elution of PPACK in a C_{18} column was achieved with an isocratic method employing 9.9% acetonitrile, .089% trifluoroacetic acid, and 90.011% water. PPACK was detected via phenylalanine absorbance (258 nm). Zeta potential measurements were used for further verification of PPACK coupling (Brookhaven Instruments).

Thrombin Inhibition Experiments

Tosyl-Gly-Pro-Arg-4 nitranilide acetate (Chromozym TH, Roche Applied Science) assay assessed PPACK inhibition of thrombin and plasmin in accordance with previously described methods[28]. 100 μL of 12 nM thrombin was incubated for 60s at room temperature with selected amounts of PPACK or PPACK-nanoparticles or with an excess of bare nanoparticles. 500 μL (100 μM) of Chromozym TH was added to terminate the PPACK-thrombin interaction. Thrombin activity against the substrate was measured via absorbance at 405 nm. Rate of change in absorbance at 405 nm indicated amount of uninhibited thrombin.

Chromozym TH assay assessed the kinetics of the PPACK-thrombin interaction. .92 nM thrombin was incubated at room temperature with 5 nM PPACK or .3 pM PPACK nanoparticles over various times prior to introduction of 500 μL of 100 μM Chromozym TH. Thrombin activity was measured as above. Kinetics of inhibition were characterized in accordance with the work of Kettner and Shaw[29]. Modeling inhibition according to equation (1), an estimate of the second order constants (k_2/K_i) for the PPACK-thrombin interaction and the PPACK nanoparticle-thrombin interaction were obtained via equation (2) following a linear fit to log(activity) versus time data to determine pseudo-first-order rate constant k_{app}. To best obtain a pseudo-first-order reaction, thrombin dilution was maximized within the limits set by the sensitivity of the assay.

$$Thrombin + PPACK \overset{K_i}{\rightleftharpoons} Reversible\ Complex \xrightarrow{k_2} Alkylated\ Thrombin \quad (1)$$

$$\frac{k_{app}}{[PPACK]} = \frac{k_2}{K_i} \ if\ [PPACK] \ll K_i \quad (2)$$

Chromozym TH assay measured PPACK and PPACK nanoparticle activity against plasmin. 120 nM Plasmin was incubated for three minutes at room temperature with PPACK or PPACK nanoparticles. 1000-fold excess (138 μM) of PPACK (free or on nanoparticles) was employed to produce a measurable effect on plasmin activity against Chromozym TH. Activity after incubation with PPACK and PPACK nanoparticles was compared.

Antithrombotic Effects In Vivo

As in previous work[28,30], 10–12 week old male C57BL/6 mice (weight 25–30 g) were subjected to photochemical injury of the carotid. After anesthetization with sodium pentobarbital, the right common carotid artery was isolated via midline cervical incision. An ultrasonic flow probe (model 0.5 VB Transonic Systems, Ithaca, NY) was applied to the

artery to measure flow for the duration of each experiment. A 1.5 mW 540 nm HeNe laser (Melles Griot, Carlsbad, CA) was focused on the artery at a distance of 6 cm. Heparin (.125 mg/kg, n=4), PPACK (12.5 mg/kg, n=7), PPACK nanoparticles (1 mL/kg, n=7), or non-functionalized nanoparticles (1 mL/kg, n=7) were administered to the tail vein as a bolus 10 minutes prior to inducing arterial thrombus through tail vein injection of photosensitive rose bengal dye (50 mg/kg; Fisher Scientific, Fair Lawn, NJ) dissolved in PBS. In additional control experiments (n=4), no treatment preceded injection of the rose bengal dye. Occlusion of the carotid artery was noted and experiments were terminated upon the stable (>5 minutes) maintenance of zero flow.

Occluded arteries were removed and preserved. For transmission electron microscopy, arteries were fixed in 2% glutaraldehyde and .1 mM sodium cacodylate at 4 degrees. Fixed tissues were stained with osmium tetroxide, tannic acid, and uranyl acetate. Tissues were then dehydrated and embedded in PolyBed 812 (Polysciences). Semi-thin sections were stained with Toluidine Blue and evaluated under light microscope for the presence of occlusive clotting. Portions of arteries identified as containing thrombi were subsequently sliced for transmission electron microscopy. Thin sections were counterstained with uranyl acetate and lead citrate. Samples were examined with a Zeiss 902 Electron Microscope and images were recorded with Kodak EM film.

For Carstair's staining to identify platelets and fibrin, arteries were preserved in 10% buffered formalin for 3 days. After processing through alcohols and xylenes, the arteries were embedded in paraffin and sectioned at 5-micron thickness. Hydrated sections were treated with 5% ferric alum, Mayer's hematoxylin, picric acid-orange G solution, poncean-fuchsin solution, 1% phosphotungstic acid, and aniline blue to stain for fibrin, platelets, collagen, muscle, and red blood cells. Images were analyzed for platelet content using ImageJ.

In additional mice, APTTs for blood obtained via left-ventricular draws were used to determine the systemic effects of the particles. Citrate-anticoagulated blood was obtained 10, 20, 40, 70, 110, or 150 minutes after injection of a bolus of PPACK nanoparticles or 10 minutes after injection of control nanoparticles or saline. Plasma was combined with APTT reagent (Beckman-Coulter/Instrumentation Laboratory) for three minutes prior to activation with calcium chloride and mechanical determination of coagulation time.

Imaging and Quantification of Nanoparticle Antithrombotics

Left (unaffected) and right (injured) arteries from six mice were reserved for analysis via magnetic resonance imaging and spectroscopy. Three of these mice received PPACK nanoparticles and three received blank nanoparticles prior to induction of thrombosis. Arteries were excised and rinsed with saline to remove retained blood prior to submersion in fixative as described above. Imaging and spectroscopy was conducted with a custom-built single-turn solenoid coil on a Varian 11.7T MR system. ^{19}F signal from nanoparticles in the artery and from a perfluorooctylbromide standard was assessed via spin echo spectroscopy (3 s pulse repetition time (TR), 2 ms echo time (TE), 256 signal averages (NT), 13.25 minute acquisition time). ^{19}F spin echo images (1.3 s TR, 12 ms TE, 512 NT, 32 phase encoding steps, 64 frequency encoding steps, 9mm×6mm×1mm field of view) were obtained to depict nanoparticle binding in the excised artery. ^{1}H spin echo images (1.5 s TR, 20 ms TE, 4 signal averages, 128 phase encoding steps, 256 frequency encoding steps, 9mm×6mm×1mm field of view, 5 .2mm slices) allowed coregistration of the fluorine images with an anatomical image of the artery.

Statistics

Significance levels were determined by two-tailed two-sample unequal variance T-tests. Error bars denoted standard error. Data fitting employed an iterative least-squares algorithm.

Results

Nanoparticle Synthesis

PFC nanoparticles were synthesized with inclusion of carboxy-terminated PEG capped lipids (Fig. 1). Via EDCI coupling, amide bonds were formed between the N-terminus of PPACK and the bare carboxyls on the particle surface. After conjugation of PPACK, nanoparticles were examined to verify stability. Precursor nanoparticles, were found via laser scattering to have a hydrodynamic diameter of 158.0 ± 2.4 nm. PPACK nanoparticles had a measured diameter of 160.5 0 ± 2.6 nm (Fig. 1s).

After PPACK coupling, a change in the composition of the lipid surface of the particles was evident via measurement of zeta potential. Prior to PPACK coupling, the particles exhibited a zeta potential of −35 0 ± 1.57 mV. After addition of PPACK, the zeta potential rose to −22.3 ± 1.57 mV, concordant with the expectation that the PPACK arginine would reduce the negative zeta potential of the non-functionalized nanoemulsions (Fig. 1s).

Following synthesis but before dialysis to remove PPACK that did not couple to the particles, the residual uncoupled PPACK in the emulsion was quantified by reverse phase liquid chromatography. For PPACK nanoparticles not subject to dialysis, HPLC analysis indicated approximately 13650 PPACK coupled to each particle. HPLC also determined the amount of PPACK not associated with the particles after dialysis and one week storage at four degrees, indicating of the good stability of the PPACK nanoparticle formulation (Fig. 2s).

Thrombin Inhibition: Kinetics and Specificity

PPACK and PPACK nanoparticle inhibition of thrombin was evaluated by measuring thrombin activity on the chromogenic substrate, Chromozym TH. After one-minute incubation with either PPACK nanoparticles or free PPACK, thrombin activity against the substrate decreased monotonically with increasing inhibitor concentration (Fig. 2a). PPACK on the nanoparticles gave a decay constant of .033 nM^{-1} and free PPACK gave a decay constant of .026 nM^{-1}, indicating no diminution of PPACK activity after conjugation to particles. Complete inhibition of thrombin activity was achieved at a 15.5 pM particle concentration, corresponding to deactivation of approximately 1000 thrombin by each particle.

Chromozym TH assay also defined the kinetics of PPACK and PPACK nanoparticle inhibition of thrombin in accordance with the model of Kettner and Shaw (Fig. 2b). For free PPACK, the pseudo-first-order rate constant, k_{app}, was measured as 1.824 min^{-1}. The second order constant for free PPACK was approximated as $k_{app}/[PPACK] = 3.65\times10^{8}$ $M^{-1}min^{-1}$ (whereas Kettner and Shaw originally found a constant of $1.20\times10^{9}M^{-1}min^{-1}$ [29]). PPACK on the nanoparticles exhibited a k_{app} of 1.848 min^{-1} and a second order constant of 4.47×10^{8} $M^{-1}min^{-1}$. The PPACK nanoparticle, considered as an inhibitor itself, exhibited a second order constant of 6.10×10^{12} $M^{-1}min^{-1}$. PPACK nanoparticles at the site of thrombotic injury thus have a kinetic advantage over free PPACK in the inhibition of thrombus formation. Furthermore, the kinetics of the PPACK-thrombin interaction showed no significant alteration with PPACK bound to nanoparticles. Without PPACK, the nanoparticles had no effect on thrombin activity.

Chromozym TH was used to test the response of plasmin activity to PPACK and PPACK nanoparticles (Fig. 3s). Greater than 80% inhibition of plasmin activity against Chromozym TH was achieved with 138 μM PPACK, both for free PPACK and particle- bound inhibitor. Conjugation of PPACK to nanoparticles constitutes an N-terminal modification to the inhibitor that does not compromise its specificity for thrombin over plasmin.

Antithombotic Efficacy in vivo

In trials of the in vivo effect of PPACK nanoparticles, thrombotic occlusion of the carotid artery was induced in C57BL/6 mice. Blood flow in the carotid steadily diminished as occlusion progressed (Fig. 4s). Time to occlusion indicated efficacy of fibrin and platelet deposition. Saline, heparin, non-functionalized nanoparticles, PPACK, or PPACK nanoparticles were administered ten minutes before inducing laser injury via injection of rose bengal dye (Fig. 3a). With saline sham treatment, carotid artery occlusion occurred at 70 ± 17 minutes after dye injection. Following a bolus of control nanoparticles, occlusion occurred at 66 ± 14 minutes. PPACK alone, despite its efficacy as a thrombin inhibitor in vitro, also exerted no apparent impact on thrombus formation in vivo, resulting in a mean occlusion time of 71 ± 19 minutes. The absence of an antithrombotic effect for PPACK accords with the expectation of a 2.9-minute reported clearance half-life and with the known in vivo instability of PPACK without protection of the N-terminus.

Heparin, however, has well-characterized antithrombotic effects and is a standard option as an anticoagulant for mediation of acute thrombus formation. Previous trials with the rose bengal thrombosis model yielded an occlusion time of 97 ± 18 minutes for heparin at a dose of .125 mg/kg animal weight[28]. Here, occlusion occurred at 102 ± 13 minutes (Fig. 3a).

Occlusion time more than doubled to 145 ± 13 minutes in the mice treated with a 1 ml/kg dose of PPACK nanoemulsion (in which the administered amount of PPACK was less than that given for trials of the free inhibitor) (Fig. 3a). As compared to a high dose of heparin, PPACK nanoparticles outperformed ($p<.001$) the established anticoagulant. Likewise, both PPACK nanoparticles ($p<.001$) and heparin ($p<.05$) extended time to occlusion of the carotid over PPACK treatment.

Activated partial thromboplastin time (APTT) for treatment with control nanoparticles did not significantly differ from APTT for saline treatment. At 10 minutes after injection of PPACK nanoparticles, coagulation time was significantly lengthened. However, blood withdrawn at 20 minutes after injection nearly matched control APTT values. Subsequent blood draws yielded APTTs that did not significantly differ from control values (Fig. 3b), indicating fast abatement of the systemic effects of the PPACK particles despite prolonged therapeutic effect. A similar time course was evident in preliminary measurements of bleeding times in the tail after administration of PPACK nanoparticles as a tail vein bolus (Fig. 5s).

^{19}F magnetic resonance imaging and spectroscopy were used to assess Perfluoro 15-Crown-5 Ether (CE) NMR signal present in selected arteries due to retention of PFC nanoparticles. Figure 4a depicts an excised occluded artery from a mouse treated with PPACK nanoparticles. In the left panel, a proton MRI illustrates a .2 mm cross-section of the artery with a dense clot in the center. A false color ^{19}F 1 mm projection image in the right panel depicts nanoparticle content in the artery. An overlay of the two images indicated strong colocalization of the particles with the clot, implying the possibility of tracking PPACK nanoparticles as they act to interrupt clot formation.

Quantitative ^{19}F spectroscopy was employed to quantify nanoparticle incorporation into clots from six mice (Fig. 4b). In mice treated with PPACK nanoparticles, injured arteries

retained .31 ± .14 fmol and unaffected arteries retained .04 ± .01 fmol nanoparticles. In mice treated with control nanoparticles, injured arteries retained .07 ± .03 fmol and uninjured arteries retained .03 ± .02 fmol.

To further elucidate the mechanism by which PPACK nanoparticles prevent thrombus formation, TEM was used to examine the microstructure of fully formed thrombi. In clots formed after treatment with PPACK nanoparticles, few degranulated platelets were observed. Furthermore, platelets in such clots were loosely associated with one another, showing no signs of the dense packing evident in well-formed platelet aggregates. Instead, a fibrin gel appeared to dominate the clot microstructure (Fig. 5a). In TEM images of clots subject to control nanoparticle treatment, close association and interdigitation of platelets was evident. Similarly, degranulated platelets were abundant in these thrombi (Fig. 5b).

Carstair's staining was used to assess relative amounts of platelets and fibrin in selected clots. Staining of clots formed after PPACK nanoparticle treatment indicated a predominance of fibrin with only sparse clusters of platelets (Fig. 6s). For clots formed in the presence of control nanoparticles, platelet staining was denser and interconnected (taking up 7.28% of clot area as opposed to 1.66% in PPACK-treated clots) (Fig. 7s).

Discussion

Prior work in our lab and others has defined the pharmacokinetics of functionalized PFC nanoparticles for drug delivery and imaging applications[16,31]. Based on these studies and the long clinical history of PFC use as a blood substitute, the *in vivo* safety and stability of the base PFC emulsion has been established. Stable attachment of covalently bound targeting ligands has also been demonstrated for this class of agents [32–34]. Building on this platform, the PPACK nanoparticle was designed as a direct thrombin inhibitor presenting a thrombin absorbing surface that is bound and retained at a site of acute thrombosis. Although PPACK itself is not clinically useful as an antithrombotic[10,35], the PPACK PFC nanoparticle is an effective anticoagulant due to sequestration of numerous PPACK ligands at the site of thrombosis that continue to maintain prolonged surveillance against any subsequently activated thrombin after the initial binding event.

To demonstrate efficacy of the particle *in vivo*, the rose bengal thrombosis model was chosen based on its known sensitivity to a wide range of anticoagulants. The standardized metric of "time to arterial occlusion" in this model has been used to examine the potency of other notable thrombin inhibitors[30]. We demonstrate that the PPACK nanoparticle can delay localized occlusive thrombosis in this model while rapidly minimizing systemic effects on bleeding times, and indeed appears more effective than a selected conventional anticlotting agent. Although PPACK is used as the active pharmaceutical ingredient in this case, the antithrombotic nanoparticle acts as a unique inhibitor in its own right regardless of the drug that is conjugated to the particle. Rather than serving simply as a vehicle that delivers and releases an antagonist to the thrombin target, the particle holds onto the inhibitor and acts against thrombus formation by maintaining localized thrombin-absorbing surfaces that are not disabled after locating a thrombin target.

Given the colocalization of the particle with sites of thrombosis and the extensive previous use of PFC particles to provide magnetic resonance, ultrasound, optical and SPECT contrast[17,27,31–34], PPACK nanoparticles exhibit promise as a tool for specific diagnostic mapping of acute thrombosis. As demonstrated previously for detection of fibrin in clots[27], ^{19}F signatures from PFC particles can be quantified in molarity to provide a gross estimate of their local concentration. As indicated by ^{19}F data, the isolation of PPACK particles at a forming thrombus establishes a focal antithrombotic surface covering the

prothrombotic nascent clot. The ability of the particles to cover the clotting surface with a thrombin-inhibiting coating could theoretically seal off further thrombus formation as PPACK on the bound particles continues to bind newly activated thrombin.

Our analysis of thrombotic occlusions formed in the presence of PPACK particles indicates that, as part of its therapeutic impact, the antithrombotic particle also impacts platelet deposition. The particle likely inhibits thrombin's ability to activate platelets via PAR cleavage[19–23]. As evaluated with Carstair's staining (Fig. 5s) and with TEM (Fig. 5), the morphology of the clots formed after PPACK particle treatment is distinguished by sparse platelet distribution and reduced density of packing. The apparent reduction in platelet deposition in our treatment suggests a possible broader clinical application for this particle platform as a combined antithrombotic and antiplatelet agent. Identification of the pathways through which the particles act against platelet activation and aggregation is a question of interest for future work.

The clinical introduction of specific and potent direct thrombin inhibitors has garnered attention in recent years. PPACK, though ineffective as an isolated molecule, was used here as a reasonably cheap, small, and non-toxic[35] agent to complex with PFC nanoparticles. However, other known thrombin inhibitors could be employed with the use of conventional and flexible conjugation schemes, given that diphospholipids with large varieties of linking groups and spacers are readily available commercially. The PFC nanoparticle thrombin inhibitor model would likely retain its noted advantages (including the ability to form antithrombotic surfaces) with adaptation to different inhibitory moieties. Investigation of other selected inhibitors, various inhibitor loadings, and particle dose dependencies would comprise future studies to advance the antithrombotic nanoparticle towards clinical use. More thorough investigation of the systemic effects of antithrombotic nanoparticles, including prothrombin time, thrombin time, platelet aggregometry, and further bleeding tests, would be necessary.

There continues to be a medical need for new potent and highly specific antithrombotic agents with minimal toxicity for the treatment of thrombosis in acute coronary syndromes[5–7], stroke[8], venous thrombosis[6,9], and stent placement[36]. We suggest that the particle developed here could be evaluated in acute vascular syndromes as a potent local therapy with an improved safety profile serving as a bridge to outpatient oral therapy.

Addendum

The authors acknowledge the contributions of Ralph Fuhrhop to the nanoparticle formulation, of Huiying Zhang and Noriko Yanaba to tissue preparation for Carstair's staining, and of Marilyn Levy to TEM image preparation.

Supplementary Material

Refer to Web version on PubMed Central for supplementary material.

References

1. Davies MJ. Anatomic features in victims of sudden coronary death. Coronary artery pathology. Circulation. 1992; 85:I19–I24. [PubMed: 1728500]
2. Furie B, Furie BC. Mechanisms of thrombus formation. The New England Journal of Medicine. 2008; 359:938–949. [PubMed: 18753650]
3. Ansell J, Hirsh J, Poller L, Bussey H, Jacobson A, Hylek E. The pharmacology and management of the vitamin K antagonists. Chest. 2004; 126:204S–233S. [PubMed: 15383473]

4. Schwartz RS, Burke A, Farb A, Kaye D, Lesser JR, Henry TD, Virmani R. Microemboli and microvascular obstruction in acute coronary thrombosis and sudden coronary death: relation to epicardial plaque histopathology. Journal of the American College of Cardiology. 2009; 54(23): 2167–2173. [PubMed: 19942088]
5. Lee LV. Anticoagulants in coronary artery disease. Clinical Cardiology. 2008; 26:615–628.
6. Turpie AG. The top four advances in antithrombotic care in the last year. Thrombosis Research. 2008; 123:S2–S6. [PubMed: 18834617]
7. Fareed J, Iqbal O, Cunanan J, Demir M, Wahi R, Clarke M, Adiguzel C, Bick R. Changing trends in anti-coagulant therapies. Are heparins and oral anticoagulants challenged? International Journal of Angiology. 2008; 27:176–192.
8. Bousser MG. Antithrombotic agents in the prevention of ischemic stroke. Cerebrovascular Diseases. 2009; 27:12–19. [PubMed: 19439936]
9. Gross P, Weitz JI. New antithrombotic drugs. Clinical Pharmacology and Therapeutics. 2009; 86:139–146. [PubMed: 19553932]
10. Kaiser B, Hauptmann J. Pharmacology of Synthetic Thrombin inhibitors of the tripeptide type. Cardiovascular Drug Reviews. 1992; 10:71–87.
11. Srivastava S, Goswami LN, Dikshit DK. Progress in the design of low molecular weight thrombin inhibitors. Medicinal Research Reviews. 2005; 25:66–92. [PubMed: 15389730]
12. Di Cera E. Thrombin. Molecular Aspects of Medicine. 2008; 29:203–254. [PubMed: 18329094]
13. Wickline, SA.; Mason, RP.; Caruthers, SD.; Chen, J.; Winter, PM.; Hughes, MS.; Lanza, GM. Fluorocarbon agents for multimodal molecular imaging and targeted therapeutics. In: Weissleder, R.; Ross, BD.; Rehemtulla, A.; Gambhir, SS., editors. Molecular imaging: principles and practice. Shelton, CT: Peoples Medical Publishing House; 2010. p. 542-573.
14. Wickline SA, Neubauer AM, Winter PM, Caruthers SD, Lanza GM. Molecular imaging and therapy of atherosclerosis with targeted nanoparticles. Journal of Magnetic Resonance Imaging. 2007; 25:667–680. [PubMed: 17347992]
15. Peters D, Kastantin M, Kotamraju VR, Karmali PP, Gujraty K, Tirrell M, Ruoslahti E. Targeting atherosclerosis by using modular, multifunctional micelles. Proceedings of the National Academy of Sciences. 2009; 106:9815–9819.
16. Flaim SF. Pharmacokinetics and side effects of perfluorocarbon-based blood substitutes. Artificial Cells, Blood Substitutes, and Immobilization Biotechnology. 1994; 22:1043–1054.
17. Winter PM, Caruthers SD, Wickline SA, Lanza GM. Molecular imaging by MRI. Current Cardiology Reports. 2006; 8:65–69. [PubMed: 16507239]
18. Bode W, Turk D, Karshikov A. The refined 1.9-Å crystal structure of D-Phe-Pro-Arg chloromethylketone-inhibited human alpha-thrombin: Structure analysis, overall structure, electrostatic properties, detailed active-site geometry, and structure-function relationships. Protein Science. 1992; 1:426–471. [PubMed: 1304349]
19. Ivey ME, Little PJ. Thrombin regulates vascular smooth muscle cell proteoglycan synthesis via PAR-1 and multiple downstream signaling pathways. Thrombosis Research. 2008; 123:288–297. [PubMed: 18571697]
20. Hirano K. The roles of proteinase-activated receptors in the vascular physiology and pathophysiology. Arteriosclerosis, Thrombosis, and Vascular Biology. 2007; 27:27–36.
21. Coughlin SR. Thrombin signaling and protease-activated receptors. Nature. 2000; 407:258–264. [PubMed: 11001069]
22. Bretschneider E, Kaufmann R, Braun M, Nowak G, Glusa E, Schrör K. Evidence for functionally active protease-activated receptor-4 (PAR-4) in human vascular smooth muscle cells. British Journal of Pharmacology. 2001; 132:1441–1446. [PubMed: 11264237]
23. Bretschneider E, Spanbroek R, Lötzer K, Habenicht AJ, Schrör K. Evidence for functionally active protease-activated receptor-3 (PAR-3) in human vascular smooth muscle cells. Journal of Thrombosis and Haemostasis. 2003; 90:704–709.
24. Davie EW, Kulman JD. An overview of the structure and function of thrombin. Semin Thromb Hemostasis. 2006; 32(Suppl 1):3–15.

25. Ghigliotti G, Waissbluth AR, Speidel C, Abendschein DR, Eisenberg PR. Prolonged activation of prothrombin on the vascular wall after arterial injury. Arterioscler Thromb Vasc Biol. 1998; 18:250–257. [PubMed: 9484990]
26. Duguid JB. Thrombosis as a factor in the pathogenesis of coronary atheroscle- rosis. J Pathol Bacterial. 1946; 58:207–212.
27. Flacke S, Fischer S, Scott MJ, Fuhrhop RJ, Allen JS, McLean M, Winter P, Sicard GA, Gaffney PJ, Wickline SA, Lanza GM. Novel MRI contrast agent for molecular imaging of fibrin: Implications for detecting vulnerable plaques. Circulation. 2001; 104:1280–1285. [PubMed: 11551880]
28. Vicente CP, He L, Pavão MSG, Tollefsen DM. Antithrombotic activity of dermatan sulfate in heparin cofactor II-deficient mice. Blood. 2004; 104:3965–3970. [PubMed: 15315969]
29. Kettner C, Shaw E. D-Phe-Pro-ArgCH_2Cl-A selective affinity label for thrombin. Thrombosis Research. 1979; 14:969–973. [PubMed: 473131]
30. Westrick RJ, Winn ME, Eitzman DT. Murine models of vascular thrombosis. Arteriosclerosis, Thrombosis, and Vascular Biology. 2007; 27:2079–2093.
31. Hu G, Lijowski M, Zhang H, Partlow KC, Caruthers SD, Kiefer G, Gulyas G, Athey P, Scott MJ, Wickline SA, Lanza GM. Imaging of vx-2 rabbit tumors with $\alpha_v\beta_3$-integrin-targeted ^{111}In nanoparticles. International Journal of Cancer. 2007; 120:1951–1957.
32. Lanza GM, Abendschein DR, Hall CS, Marsh JN, Scott MJ, Scherrer DE, Wickline SA. Molecular Imaging of Stretch-Induced Tissue Factor Expression in Carotid Arteries with Intravascular Ultrasound. Investigative Radiology. 2000; 35(4):227–234. [PubMed: 10764091]
33. Winter PM, Caruthers SD, Kassner A, Harris TD, Chinen LK, Allen JS, Lacy EK, Zhang H, Robertson JD, Wickline SA, Lanza GM. Molecular Imaging of Angiogenesis in Nascent Vx-2 Rabbit Tumors Using a Novel $\alpha_v\beta_3$ targeted Nanoparticle and 1.5 Tesla Magnetic Resonance Imaging. Cancer Research. 2003; 63:5838–5843. [PubMed: 14522907]
34. Winter PM, Morawski AM, Caruthers SD, Fuhrhop RM, Zhang H, Williams TA, Allen JS, Lacy EK, Robertson JD, Lanza GM, Wickline SA. Molecular Imaging of Angiogenesis in Early-Stage Atherosclerosis with $\alpha_v\beta_3$ Integrin-Targeted Nanoparticles. Circulation. 2003; 108:2270–2274. [PubMed: 14557370]
35. Collen D, Matsuo O, Stassen JM, Kettner C, Shaw E. In vivo studies of a synthetic inhibitor of thrombin. Journal of Laboratory and Clinical Medicine. 1982; 99:76–83. [PubMed: 7054350]
36. Kukreja N, Onuma Y, Daemen J, Serruys PW. The future of drug-eluting stents. Pharmacological Research. 2008; 57:171–180. [PubMed: 18339557]

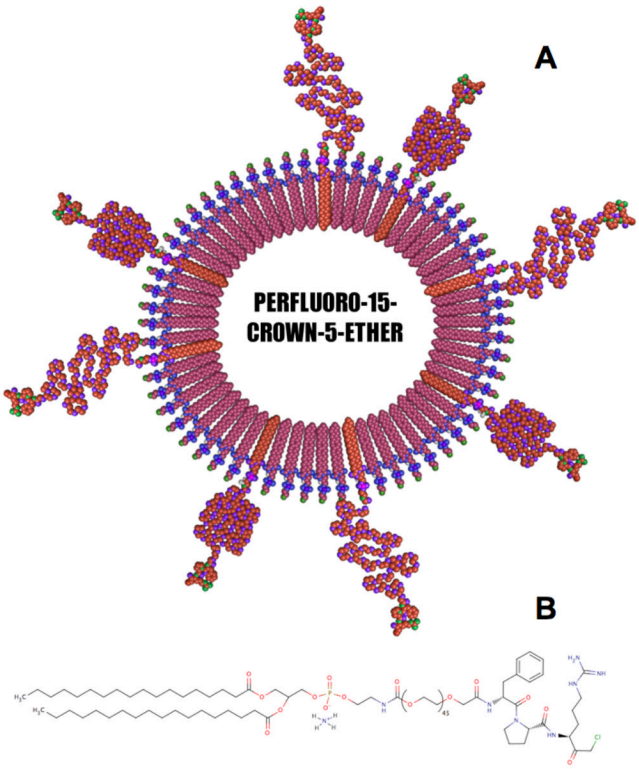

Figure 1.

Schematic of the PPACK-functionalized PFC-core nanoparticle **(a)**. The majority of the phospholipid monolayer comprised an egg lecithin L-α-phosphatidylethanolamine layer. 1% of the lipid film was 1,2-distearoyl-sn-glycero-3-phosphoethanolamine-N-[carboxy(polyethylene glycol)-2000], functionalized with PPACK after particle synthesis **(b)**.

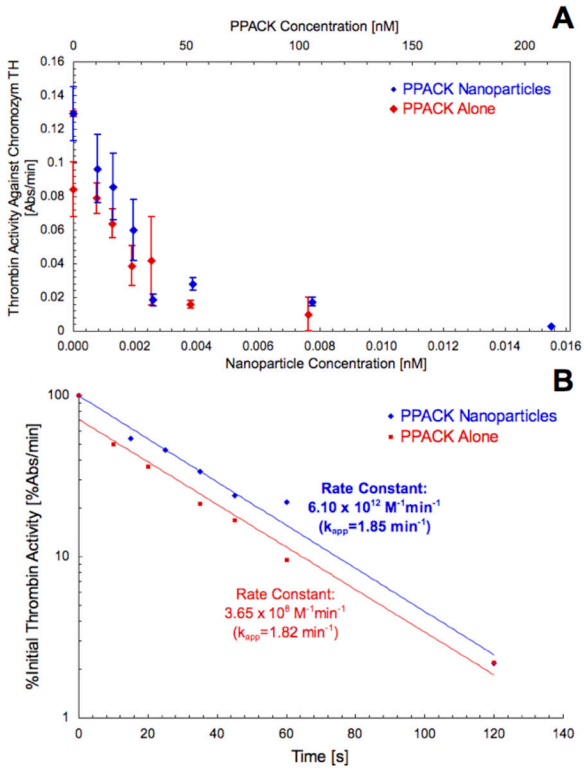

Figure 2.

PPACK caused concentration-dependent inhibition of thrombin activity against Chromozym TH. For PPACK-nanoparticles, the dependence of thrombin activity on PPACK concentration was identical to that for free PPACK, accordingly indicating greater antithrombin activity per particle than per individual free PPACK **(a)**. Study of the kinetics of thrombin inhibition indicated no modification to PPACK activity against thrombin after placement on nanoparticles **(b)**. For .93 nM thrombin and 5 nM PPACK (.0003 nM PPACK-nanoparticles), PPACK exhibited a second order constant (k_2/K_I) of 3.65×10^8 $M^{-1}min^{-1}$ and PPACK-nanoparticles exhibited a second order constant of 6.10×10^{12} $M^{-1}min^{-1}$ (corresponding to 4.47×10^8 $M^{-1}min^{-1}$ for PPACK on the particles).

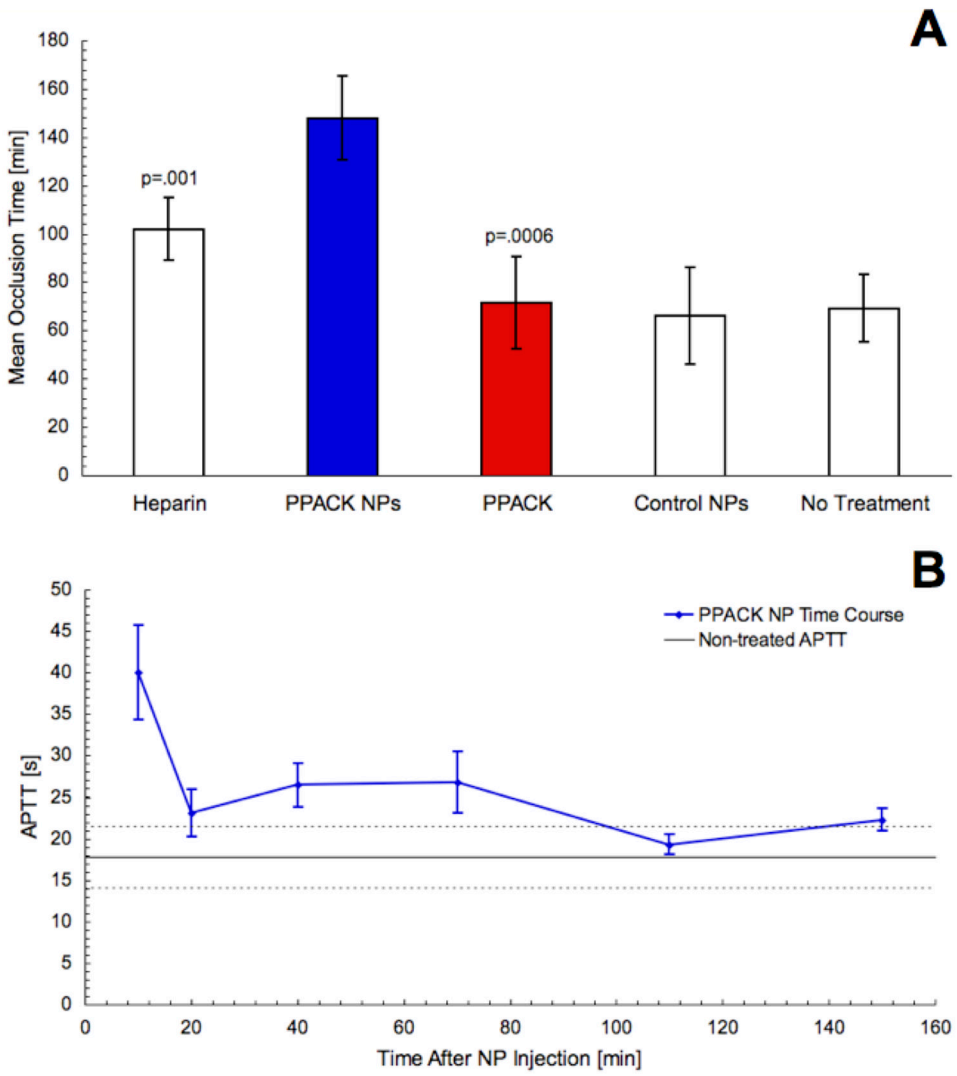

Figure 3.

Mean ± standard deviation occlusion time for each tested treatment condition in photochemical thrombotic injury experiments. Treatment with PPACK (n=7) or non-functionalized nanoparticles (n=7) did not delay occlusion time. PPACK-nanoparticle treatment more than doubled occlusion time over PPACK-treated (p=.0006) or non-treated mice (n=7). PPACK-nanoparticle treatment also lengthened occlusion time relative to heparin treatment (p=.001, n=4) **(a)**. In blood draws, PPACK nanoparticles delayed the APTT only briefly, with systemic coagulation times approaching control values over the first 20 minutes after injection **(b)**.

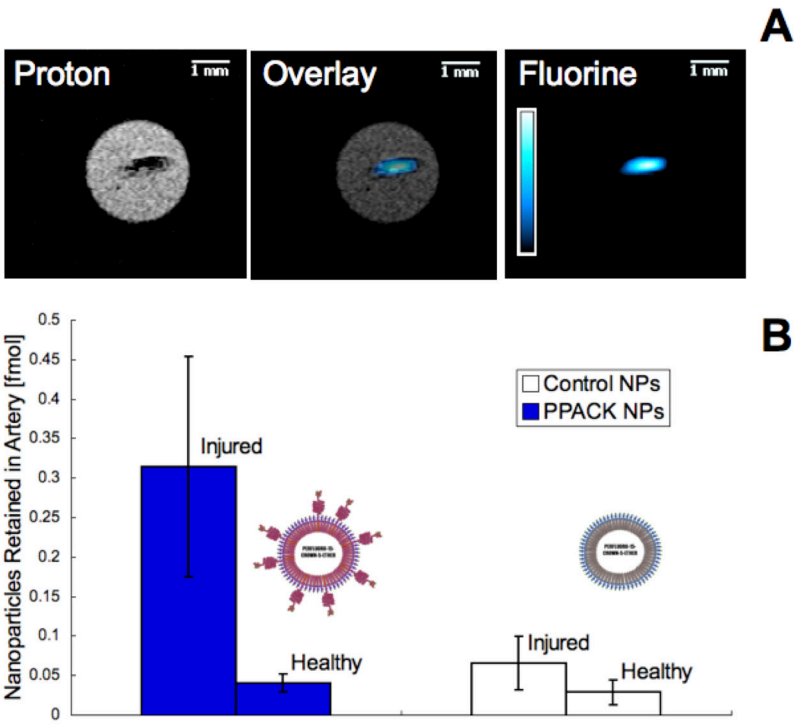

Figure 4.

In mice receiving treatment with control nanoparticles (n=3) or PPACK nanoparticles (n=3), both carotid arteries were excised following induction of occlusive thrombi in the right carotid artery. ^{19}F MRI at 11.7T exhibited coregistration of ^{19}F signal from PPACK nanoparticles with ^{1}H images depicting the occlusive clot in the artery (**a**). ^{19}F MRS was used to quantify retention of nanoparticles in the injured right carotid artery (RA) and the unharmed left carotid artery (LA). Retained particles ± standard error are represented in (**b**).

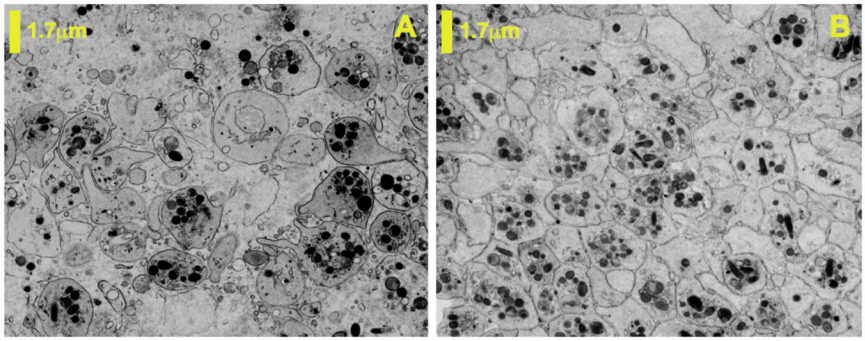

Figure 5.

TEM was used to characterize microstructure of excised clots formed during PPACK nanoparticle or control nanoparticle treatment. Clots formed in the presence of PPACK-nanoparticles had loosely associated platelets with little evidence of degranulation **(a)**. Close association, degranulation, and interdigitation of platelets was evident in clots formed in the presence of control nanoparticles **(b)**.